Laboratory Investigation on Seams between Rails and Hardened Fine-grained, as well as Hadfield Steel Plates with Manual Arc Welding

András Brautigam[1,3], Szabolcs Szalai[2,3], Nikoletta Légmán[2,3], Szabolcs Fischer[2,3,*]

[1]Budapest Transport Privately Held Corporation (BKV)
Akácfa u. 15, H-1072 Budapest, Hungary
brautigama@bkv.hu

[2]Széchenyi István University, Central Campus Győr
Egyetem tér 1, H-9026 Győr, Hungary
{szalaisz,legman.nikoletta,fischersz}@sze.hu

[3]Széchenyi István University, Vehicle Industry Research Center
Egyetem tér 1, H-9026 Győr, Hungary
[*]Corresponding author e-mail: fischersz@sze.hu

Abstract: In the last decade, hardened fine-grained plate components have been used in turnouts and crossings on Western European urban rail networks, as well as in Hungary, in place of traditional rail or Hadfield steel components. The first crossing was built in Hungary in 2016. These components have many advantages, such as the ease with which they can be machined in the factory; they are less prone to cracking than rails due to their block design (high load-bearing cross-section); however, their weldability to rails and lifetime repairability present numerous challenges for railway turnout manufacturers and operators. There have been numerous studies on joint and repair welding of rails and hardened fine-grained materials, but there is little or no information available on joint welding with manual arc welding of these two different materials. The current study aims to investigate the welds of coated electrode manual arc welding of rails (R260 and R400 HT) and hardened fine-grained plates (in this case, Hardox 500) under non-laboratory conditions while strictly adhering to technological specifications, in comparison to manual arc welding of rails and Hadfield steels. Laboratory tests included raw material chemical composition, macroscopic tests, micro-hardness measurements, tensile, shear, and bending tests.

Keywords: Rail; Head-special hardened rail; Hardened fine-grained plates; Joint welding; Hardox 500; Hadfield steel; Manual arc welding; Laboratory experiments

1 Introduction

Public railways and tramways are essential for sustainable urban and intercity transportation. These networks provide energy-efficient and environmentally friendly mass transit alternatives to roads [1] [2]. Urban congestion, road wear, and vehicle emissions can be reduced by using railways [3]. Civil engineers design, build, and maintain rail infrastructure to meet changing mobility demands in this complex engineering landscape. It entails integrating these systems into urban settings, ensuring environmental resilience, and making them accessible to all users. Rail dampers reduce noise and vibration, helping to meet urban environmental standards [4] [5]. Civil engineering improves railroad quality and sustainability [6] [7]. Civil engineering alone is sometimes insufficient for maintaining and constructing fixed rail systems, i.e., a more complex viewpoint is required. Mechanical engineers and material scientists collaborate with civil engineers to address complex rail system structural deterioration issues such as wheel-rail interaction [8]. Material scientists evaluate rail-stress-resistant materials, whereas mechanical engineers investigate moving systems. Optimizing rail operations for multiple modes improves network capacity and reliability. This collaboration is required to construct international rail transport infrastructure, overcome logistical and regulatory barriers to cross-border movement, and ensure global trade and connectivity [9, 10]. Material scientists, mechanical engineers, and civil engineers create energy-efficient fixed rail systems [11]. This collaboration predicts and improves rail components such as ballast using advanced simulation and novel materials to increase infrastructure durability and operational life [12-15]. A multidisciplinary team tackles international transportation logistics and sustainable urban growth, making rail transport more appealing to both freight and passengers [9] [10]. Civil engineers, mechanical engineers, and material scientists shape sustainable mobility and urban development as societies seek environmentally friendly transportation and solutions to urban congestion and pollution.

The topic of the current paper is related to special rail welding for turnouts and crossings. Below, the authors collected relevant information on the background of this area.

Before analyzing the welding results, examining the geometry of the turnouts and crossings [16] made of hardened fine-grained plates is advisable. In most cases, the same structural height as the rails can be achieved by attaching, e.g., a 55-mm thick hardened fine-grained plate to a 94-mm high structural steel base plate for a Vignol rail with 149 mm height. Such a structural design is illustrated in Figure 1 for an "open" track, where Vignol MÁV 48,5 rails are connected to the plates. Figure 2 shows that the whole structure is placed on a 20-mm thick ground plate, on which the rail is also mounted.

Figure 1
Turnouts and crossings made of hardened fine-grained plates on tramway line #59 in Budapest

Figure 2
Parts of the hardened fine-grained plates (blocks)

In many cases, the failure mechanisms occur within six months to a year of installation for medium load lines (2.5-5.0 MGT/year, where MGT means million gross tons as through-rolled axle tons) after 1.2-1.5 MGT, and for heavy load lines (5.0-7.5 MGT/year) after 2.5-3.0 MGT. Cracks appear in the heat-affected zone of the rail side, which then develop into a full cross-section fracture (Figure 3). The possibility of large openings is managed by using fasteners to prevent horizontal displacement, but repairing the fractures after installation is an extreme challenge for manufacturers and operators.

Figure 3
Cracks and fractures between the rails and the blocks

Several attempts have been made to solve this problem, either by entire cross-section welding or the solutions shown in the pictures below (Figure 4). The left and middle subfigures show the repair of a crack starting at the rail base, which, after penetration testing, clearly shows that the crack has already started to propagate down the web toward the rail head.

Figure 4
Repair welding and rail change on the blocks

The complete repair of this in the track has not been solved yet. The subfigure on the right in Figure 4 shows the replacement of a new rail where assuming that the web is complicated to weld, the web is curved, and only the foot and the rail head are welded to the block. The authors' research involves welding between different rail steel grades and hardened fine-grained plates under strict technological conditions (circumstances) in order to investigate the suitability of the welded joints in railway tracks by laboratory tests, which are compared with the results of manual joint welding of rails and Hadfield steels.

Boyan An et al. [17] investigated the track's geometric requirements and importance and found that the track rail's deviation causes high-frequency excitation in the wheel-rail interaction, leading to track deterioration. Their 3D finite element method can simulate contact geometry up to 400 km/h, which they use to determine the depths of interaction as a function of speed categories. 3D finite element simulations have also been performed by Gao et al. [18], who also investigated the stresses during rolling contact and the surface treatment of the material with plasma. The effect of the treatment can significantly reduce the wear of the rails; however, stress concentrations can develop at the grain boundaries, which increase the shear stresses in the heat-affected zone. Also, plasma surface hardening of railway rails was investigated by Xiang et al. [19], who were able to increase the wear resistance as a result of the treatment; however, the microstructure of the rail in the heat-affected zone shifted from the perlite to the martensite-banitic-bearing austenitic zone, which caused a significant hardening (750-900 HV10 > 650 HB, where HV means Vickers hardness, HB means Brinell hardness). The average width of the heat-affected zone ranged from 0.55-0.8 mm.

Barna et al. [20] investigated the hardness and microstructure in the heat-affected zone (HAZ) of rail joint welds, finding that the stress peak in the HAZ is 50 mm from the weld, and also investigated grain expansion and microstructural changes in the rail head, such as partial austenization. Fischer et al. [21] investigated the welding of different rail steel grades and investigated two-step rail quality jumps without transition welds. Their results showed both critically hard and annealed sections occurring in HAZ. Brautigam et al. [22] investigated austenitic filler materials to repair running surface defects in normal and heat-treated rails, and the conditions and circumstances for applying the technology have been established.

The mechanical properties, manufacturing, and machining of Hadfield steels have been investigated by Zellagui et al. [23], which are steels with 1-1.4% C (carbon) and 11-14% Mn (manganese) content, high tensile strength, appropriate high wear resistance, and work hardening properties. During their production, the prevention of forming carbides on the grain boundaries should be avoided, which can be achieved by rapid water cooling. If the microstructure is not purely austenitic, but carbides have formed in the austenitic matrix on the grain boundaries, these carbides can reduce the steel's toughness, ductility, and brittleness. The avoidance of carbide formation was also studied by Wahyudi et al. [24], who investigated the formation of carbides at different austenization temperatures. He found that the higher the temperature, the larger the grains formed.

Venturelli et al. [25] investigated the effect of different Mn contents (5-8-12-15-18%) on the wear of Hadfield steels, finding that steels with 15% Mn content have the best post-work value (249 J) and also the highest micro-hardness value (HV30).

Laboratory testing of Hardox plates has been the subject of several studies. Ligier et al. [26] compared the wear resistance of three different commercially available Hardox steels at three different abrasive loads and found the relative wear properties of the Hardox plates. The Hardox 600 plate showed one-third less wear than the Hardox 500 plate. The effects of different heat treatment processes on Hardox sheets were investigated by Gallina et al. [27], who compared the properties of Hardox 500 with STRENX 700. The plates were subjected to various heat treatment processes, such as hardening, tempering, and normalization. In the case of tempering and normalization, the initial hardness of 500 HB is reduced to 300 HB or below.

The cutting parameters of Hardox plates were investigated by Émerson S. Passari et al. [28], who determined the optimal parameters for cutting to minimize tool wear. The most crucial parameter in the model was the depth of the cut.

The above studies illustrate that there is already a large amount of research available on the materials individually. However, there is no or minimal information available on the bonding of these different materials, so it is necessary to investigate them.

In urban railway tracks, the following base materials are the most common for hardened fine-grained plates (plate thickness >40 mm), as illustrated in Table 1.

Table 1 also indicates the chemical composition of the rails according to EN 13674-1 [29] and Hadfield steels used in the tests.

Table 1

Chemical composition and hardness values of the most common base materials

Base material	**Chemical composition [g/g %]*,****									**Hard-ness [HB]**
	C	Mn	Si	P	S	Cr	Mo	Ti	Ni	
R260	0.60-0.82	0.65-1.25	0.13-0.60	0.03	0.03	0.15	0.02	0.025	NA	260-300
R400 HT	0.88-1.07	0.95-1.35	0.18-0.62	0.025	0.025	0.03	0.02	0.025	NA	400-440
Raex 400	0.23	1.70	0.80	0.025	0.015	1.50	0.50	NA	1.00	360-440
Durostat 400	0.15	2.30	0.60	0.025	0.010	0.50	0.20	0.050	NA	360-440
Hardox 400	0.32	1.60	0.70	0.025	0.010	2.50	0.60	NA	1.50	370-430
Hardox 450	0.26	1.60	0.70	0.025	0.010	1.40	0.60	NA	1.50	425-475
Hardox 500	0.30	1.30	0.40	0.020	0.010	2.20	0.40	NA	2.0	470-530
Hadfield	1.22	12.50	0.40	NA	NA	NA	NA	NA	NA	200***

* Where there is no given range, the values mean ultimate values.

** NA means no requirement available

*** Hardens by shaping

The base materials for the welds have the following chemical composition (Table 2) according to the spectrometer tests with the WAS Foundry Master machine and WASLAB software. It is worth mentioning that the chemical content of boron was less than 0.001% in each tested base material.

Table 2

Average chemical composition of the used base materials according to spectrometer tests

Base material	**Chemical composition [%]**									
	C	Mn	Si	P	S	Cr	V	Mo	Ti	Ni
R260	0.748	0.842	0.227	0.010	0.014	0.015	<0.002	<0.005	<0.002	0.013
R400HT	0.897	1.180	0.333	0.010	0.013	0.198	<0.002	<0.005	<0.002	0.029
Hardox	0.271	0.679	0.258	0.010	0.005	0.621	0.013	0.032	0.004	0.070
Hadfield	1.100	12.900	0.306	0.017	0.003	0.098	<0.002	0.015	NA	0.082

Given that the geometry of these structures is completely different from the connecting rails, the welding processes used in previous designs, such as thermit welding or flash butt welding, are not an option here. Instead, only manual arc welding procedures (e.g., 111 means manual metal arc welding, 114 means self-shielded tubular cored arc welding, and 135 means MAG /Metal active gas/ welding with solid wire electrode according to EN ISO 4063:2023 [30]) can be used to produce the welds. The first two procedures should be used in the railway track,

while in operational conditions, the 135 procedure is preferable, as the shielding gas must be protected from weather conditions, such as the wind outdoors. It is evident from the above that there is also a risk of weld failure from human factors in manual arc welding, compared to flash butt welding. A further complicating factor is the need to weld three different materials in one cross-section, typically requiring three separate filler metals and technologies.

2 Materials and Methods

Vignol 54E1 profile R260 and R400 HT rails were applied for the tests to investigate the joint welds on normal and heat-treated rails. Given the different cross-sectional profile shapes and the expected laboratory tests, the authors had to machine the rails into plate sections, which was achieved by using the foot and web of the rails to weld the Hardox and Hadfield plates together.

Cutting off the rounded parts of the foot of the rails, a 12 mm thick "plate" could be cut out, while the web of the rails was 15 mm thick. The authors combined 12 and 15-mm thick Hardox and 12-mm thick Hadfield steel plates to this piece. Before performing the welds, the following points were taken into account:

- The welds should be reproducible
- They should be capable of being carried out both in the factory and in the railway track (given that the welding conditions in the track are complex, it has to be continued to define further criteria along these lines)
- The technology used must be well-defined
- The materials used should be easily identifiable and accessible, adapted to the diameters and chemical composition used in the railway sector
- Single V welds for equal fusion, and due to the used electrode diameter,
- Preheating of different base materials according to technology and use of interpass temperatures
- Electrode conduction (pulling) due to slag formation to avoid slag under the weld and to allow slag removal

Based on the available operational experiences, it was decided to use austenitic filler metals with a high elongation compared to the base materials. However, given that these materials harden under traffic (condition), the application of different groups of materials on the running surface would result in parts of different hardening processes (harder and softer than the base material) in and around the weld, which would also lead to accelerated aging at the most critical point. Therefore, cases were also investigated where a hard-facing layer of the same hardness as the rail base material on one side is welded on the running surface (top 6-8 mm of the plate).

To this aim, a total of two test plates (the approx. sizes are written later) per process were welded for six different processes using manual metal arc welding (Table 3). Given that Hadfield steels are work-hardening materials, as are the austenitic filler metals used, no hard-facing layer was applied to the running surface when welding Hadfield steels to rails (Table 4).

Table 3
Welding processes with the main parameters

Nr.	Base mat. #1	Base mat. #2	Filler metal	Weld. pr.
#1	R260	Hardox 500	fully austenitic	111
#2	R260	Hardox 500	austenitic + hard surfacing layer	111
#3	R400 HT	Hardox 500	fully austenitic	111
#4	R400 HT	Hardox 500	austenitic + hard surfacing layer	111
#5	R260	Hadfield	fully austenitic	111
#6	R400 HT	Hadfield	fully austenitic	111

The welds were not carried out under factory conditions but in a workshop in order to make the conditions for welding in the field as similar as possible. Accordingly, the preheating was performed with the same high-power preheating guns used in the railway track, and the other equipment used for welding was the same as that used for railway track welding. The plates and filler metals were prepared as shown in Figure 5 (left), with the lengths marked every 5 cm on the electrodes to provide the data for any potential calculations (e.g., heat input).

Table 4
Main parameters of the used filler metals

Nr.	Type	Class according to EN 14700 [31]	Chemical composition %					Dia-meter [mm]	Current [A]
			C	Si	Mn	Cr	Ni		
#1	austenitic	E Fe10	0.1	0.8	6.0	19.0	9.0	4.0	130-180
#2	Hard-facing R260	E Fe1	0.15	1.1	1.2	0.8	NA	5.0	180-230
#3	Hard-facing R400 HT	E Fe1	0.2	0.5	0.40	2.8	NA	5.0	170-240

Due to the characteristics of the plates and the equipment, two technological parameters had to be deviated from the track welds. In order to weld the root weld with the 4 mm diameter electrode, a 3 mm root tape was used and the plates had to be turned in the first round to make the root weld. The 3 mm root tape may seem like a lot compared to the thickness of the plates, but with this size, it can be guaranteed that the root seam would not break. However, the disadvantage was that the root was less likely to melt through, which had to be machined out after the plates were turned. The deformations caused by the heat input by lifting the plates had to be compensated (Figure 5, right). The extent of this was determined in advance by test welds on small pieces. The dimensions of the plates were approximately 150×350 mm.


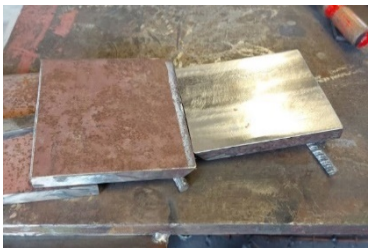

Figure 5
Plates and electrodes prepared for welding (left), lifting of the plate's edges to compensate the heat input (right)

After the root was completed, the plates were returned and preloaded, and in order to fit the 4 mm diameter electrode between the plates, the root had to be machined, as shown in Figure 6 (left and middle). At this point, there was a slight deviation from the orbital welds, as a large part of the root weld had to be ground out to allow the coated electrode to fit into the gap (Figure 6, right). For smaller diameter electrodes, which are not common on railway tracks, it would have been sufficient to blow out the gap with compressed air after slagging or grind it with a 3-mm-thick disc.

Figure 6
Machining the root on the preloaded plates (left and middle), fitting the 4 mm electrode between the plates (right)

For the reasons mentioned above, the single V-weld design was chosen, while in track, it would be more practical to use half V-weld with a 45-60° bevel on the side of the rail so that the plate does not have to be cut out, but still allows for sufficient fusion when turning on the block during welding.

As the welds were produced, the appropriate degree of preheating was carried out sequentially, followed by welding the weld lines. The preheating and interpass temperatures were continuously measured using a contact thermometer, the technologically necessary cool-down times were always waited for, and only then was reheating done if necessary (Figure 7). Each row has been slagged and cleaned with a grinding disc. The preheating and interpass temperatures for each material were as follows (Table 5). The exact welding parameters cannot be determined due to the limited space, i.e., Tables 3-4 contain further details (e.g., ranges).

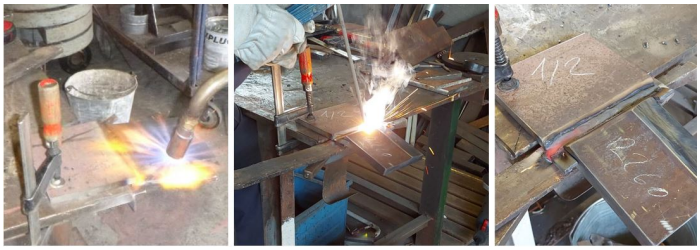

Figure 7
Welding progress (preheating, welding)

Table 5
Preheating and interpass temperatures for the base materials

Base material	**preheating temperature [°C]**	**interpass temperature [°C]**
R260 rail	300-350	300
R400 HT rail	350-400	300-350
Hardox	75-125	max. 225
Hadfield	none	max. 200

The finished test plates, illustrated in Figure 8, were prepared for laboratory testing by milling and cutting after welding. First, the edges of the plates were removed by milling, and then any not wholly flat plates were milled down to a uniform thickness of about 10 mm. This was followed by longitudinal cutting of the plates and then re-milling the rectangular specimens on all four sides to remove any hardened and uneven areas that may have been created during cutting. For the tests, samples of approximately 10×10 mm were taken. About 8-9 specimens could be machined from one pair of plates, so a total of about 16-17 specimens could be machined from two pairs of plates per process. In the laboratory tests, 2-2 specimens were used for hardness measurement and macroscopic examination, 2-2 specimens for tensile (labeled A and B), 3-3 specimens (C, D, E) for bending, and 2-2 specimens (F, G) for shearing. The remaining specimens were isolated for further testing at a later stage, e.g., microscopy or fatigue testing. The average dimensions of the specimens were 10×10×300 mm (this size is not standardized; however, the authors wanted to apply the same for all laboratory tests).

Figure 8
Milling and cutting of the plates for the laboratory tests

3 Results and Discussion

For the metallographic analyses (macrostructure and hardness measurements), specimens of 300 mm length were cut into pieces of about 70-80 mm length so that the weld, heat-affected zone, and base material could be easily examined. To prepare the surface for hardness measurement, abrasive discs of progressively finer grain size were used in several steps with continuous water cooling, followed by polishing with a 3-micron diamond suspension (Figure 9) with the following machine: Buehler Beta grinder polisher (grinding period 20-30 s, polishing period 30-60 s, adjustable clamping force 30 N). In addition, for macroscopic examinations, the specimens had to be etched, nital (nitric acid, i.e., HNO_3+alcohol) etchant was used for the rails and Hardox plates, while ammonium molybdenite (i.e., $(NH_4)_6Mo_7O_{24}$) etchant was used for the austenitic Hadfield steel and the welds. The duration of the etchings was 2-5 s.

Figure 9
Preparing the specimens for micro-hardness measurements

The width of zones was clearly visible with a microscope (Zeiss Stereo Discovery V20 with the Axio Vision software), as shown in Figures 10-12. The values in Table 6 show that with the increase in rail quality, which also brought with it an increase in preheating and interpass temperatures, the width of the thermal effect zones increased due to the heat input, with an average increase of 2-3 mm for R260-R400 HT rails, which represents an increase of 50-65%. Figures 10-12 also show the different etching patterns of the different macrostructures, as well as the design of the overlapping seams and their absence of cracks and pores.

Table 6
Length of the visible HAZ on each process

Length of the HAZ	**Rail side**	**Hardox/Hadfield side**
	average in [mm]	
Process #1	4.55	4.43
Process #2	4.58	4.36
Process #3	6.25	4.14
Process #4	7.49	4.78
Process #5	4.18	0.00
Process #6	6.23	0.00

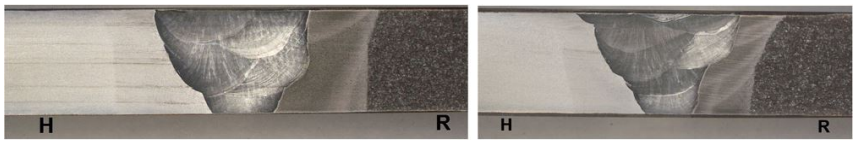

Figure 10
Macrostructural picture of processes #1 (left side) and #2 (right side)

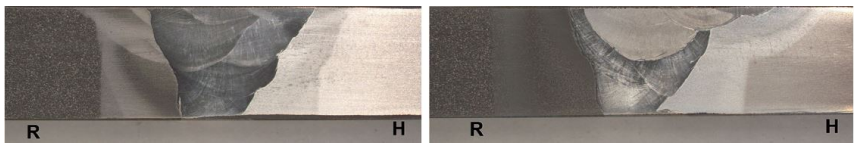

Figure 11
Macrostructural picture of processes #3 (left side) and #4 (right side)

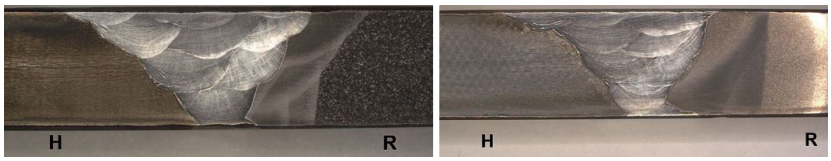

Figure 12
Macrostructural picture of processes #5 (left side) and #6 (right side)

The hardness tests were carried out according to the following standards: EN ISO 9015 [32] and EN ISO 6507 [33]. For the tests, the computer software first scanned the specimen to be tested, on which the measuring locations were marked. For both the face and the root side, the points were selected as follows: 3 to 3 measurement points in the base materials, 3 to 3 measurement points in the heat-affected zones of the base materials, and three measurement points in the weld, resulting in 15 to 15 measurement points per side, for a total of 30 points per specimen (Figure 13). The device was the KB 30 BVZ machine with KB Hardwin XL software.

The measuring device gave the values in the HV10 unit; therefore, the measurement results were converted to an HB unit based on ISO 18265:2014 [34].

The measurement results are evaluated in Figure 14 and Table 7, listed by processes. Except for process #4, the average values for the face and root side are shown, as there was no significant difference between the two sets of measurements. However, for process #4, the root and face sides welded with the hard-facing layer are also shown separately, where the peaks (436-497 HB) are clearly visible. The results also show that, even when welded with the highest technological discipline, the Hardox 500 plates anneal under the effect of the applied heat, between 307 and 391 HB values, with the lower values being closer to the weld in all cases, indicating annealing under the effect of the applied heat. In the case of

Hadfield plates, there is practically no significant difference between the heat-affected zone values of the base material and the Hadfield plate side (values between 339-361 HB for process #5 and 226-240 HB for process #6), which is due to the base material and the filler metal having almost the same chemical composition. However, for processes #5 and #6, there is a significant difference between the hardness values of the two base materials of about 120 HB, even though they are made from the same plates, also due to the amount of heat input and the resulting annealing in the case of R260 and R400 HT rails. No annealing or hardening was observed for the R260 rail, with hardness values between 257-271 HB. Considering that only the head of the R400 HT rail is heat-treated so that the web and the foot of the rail from which the specimens were machined do not reach 400 HB, only the hardness values resulting from the chemical composition of the raw material ranged from 278 to 315 HB, no significant softening was observed towards the weld. The hard-facing layer used in process #4, mixed with the high carbon content of the base material, exceeded the hardness value of 400 HB significantly.

For the destructive tests (tensile, bending, shearing), an Instron 5582 universal tensile testing machine was applied (Figure 15). Prior to the tests, the exact dimensions of the specimens were measured and recorded in the computer (Bluehill 4.42) software, and the corresponding material designation and identification number were assigned to each side; in the case of bending and shearing, the root side was underneath (pulled side), in correspondence with the position in the railway track. The machine's operating range is 2 N-100 kN in terms of applied force and 0.05-500 mm/min in speed. The tensile testing machine is also equipped with an AVE (video extensometer) system, which allows for more accurate measurements during tensile testing, as the displacement of the measuring points marked on the test specimens is recorded as opposed to the displacement of the gripping device (Figure 20).

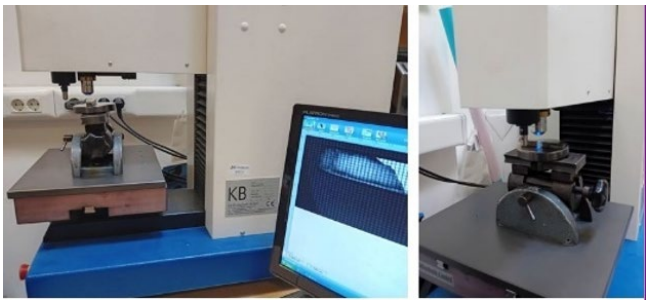

Figure 13
Micro-hardness measurement tests (instruments and specimens)

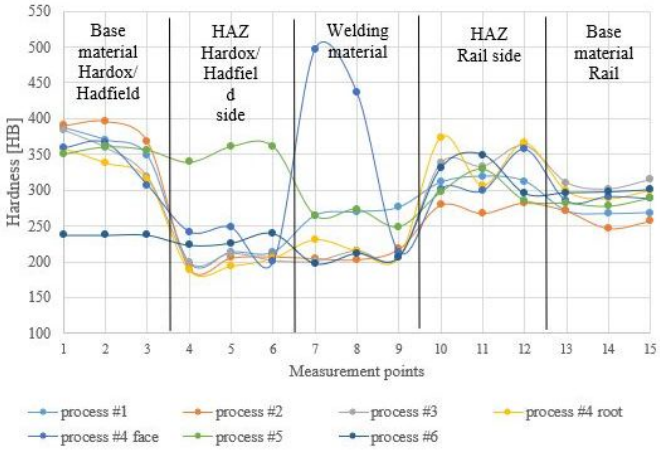

Figure 14
Hardness measurement results

Table 7
Hardness measurement results in HB unit

Process	BM_H			HAZ			VM			HAZ			BM_R		
	1	2	3	4	5	6	7	8	9	10	11	12	13	14	15
#1	388	371	348	198	213	213	265	270	276	311	320	313	271	267	269
#2	391	397	368	191	206	208	205	204	218	280	268	283	271	247	257
#3	384	359	318	199	212	202	201	215	206	338	333	362	311	302	315
#4, root	359	366	307	242	248	200	497	436	214	302	299	357	285	291	288
#4, face	358	338	315	188	194	205	231	215	206	374	307	366	299	288	300
#5	351	361	356	339	361	361	265	274	249	298	330	286	282	278	289
#6	237	237	237	223	226	240	198	212	207	331	350	296	297	298	301

Figure 15
Instron 5582 universal tensile testing machine during the tensile tests

The results (Figure 16) show that process #3 (without hard-facing layer) with R400 HT rails has the highest tensile strength (702-710 MPa) and elongation at break (4.49-4.64%), which is not surprising given the tensile strength of R400 HT rails, but method 4 with hard-facing layer shows a much more unfavorable picture, tensile strength values were reduced by more than half compared to process #3, while elongation at break values was reduced by nearly one-sixth. Process #3 is closely followed by processes #1 and #2 with an average tensile strength of 670-695 MPa, but the effect of the hard-facing layer is also felt in process #2, with an average elongation at break of 3.17%, while process #1 had 4.15%, which is closer to the maximum elongation values of process #3. Approximately 100 MPa lower tensile strength values were for Hadfield steel specimens than in process #3, but the 4% elongation at break values is already favorable considering the test results. In all cases, the tensile strength results were well below the values given in the manufacturer's data sheets for the base materials (900-1200-1400 MPa).

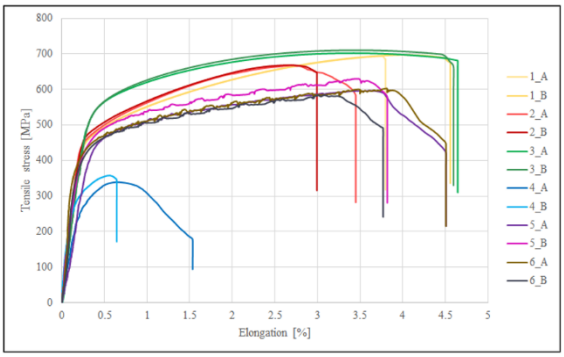

Specimen serial number	Tensile strength [MPa]	Elongation [%]
1_A	693.21	3.79
1_B	697.16	4.50
2_A	667.79	3.38
2_B	668.41	2.96
3_A	701.84	4.64
3_B	710.15	4.49
4_A	267.09	0.86
4_B	357.86	0.59
5_A	596.24	4.23
5_B	629.77	3.68
6_A	602.78	4.39
6_B	583.79	3.73

Figure 16
Results of the tensile stress tests (the number in the specimen serial number refers to the welding process)

In the bending tests, a 4-point bending arrangement (with 50-50-50 mm spacing) was chosen to ensure that only pure shear (no bending) occurs at the middle 50 mm. The arrangement is shown in Figure 17.

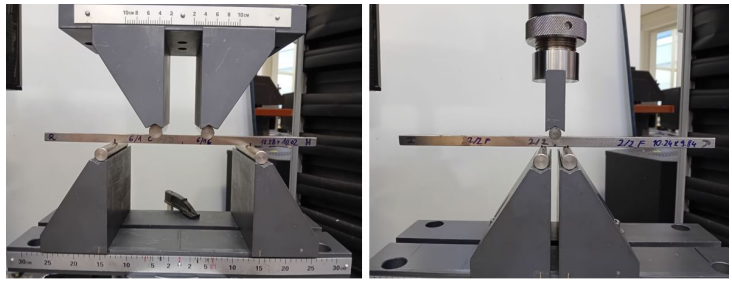

Figure 17
Test arrangement for bending (left) and shearing (right)

Also, for the bending tests (Figure 18), processes #2 and #3 showed the highest bending force values (averaging between 8.43-8.64 kN), but process #3 achieved this value at about half the displacement. After that, the values ranged from 6.4 to 7.0 kN for the other four processes, in the following decreasing order: process #4-#6 and #1. The inelasticity of the specimens in process #4 was also shown here, as only 4.87 mm average displacement could be measured, while the other processes gave average values between 13- and 35-mm. Process #1 gave the most significant displacement, with a value of more than 30 mm. The tests were not carried out until the complete fracture but up to the appearance of the first crack.

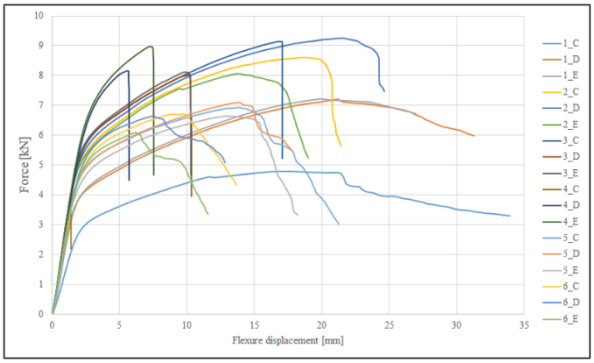

Specimen serial number	Force [kN]	Displacement [mm]
1_C	4.80	33.94
1_D	7.21	31.29
1_E	7.22	26.97
2_C	8.61	21.38
2_D	9.25	24.62
2_E	8.06	18.99
3_C	9.15	17.06
3_D	8.03	10.34
3_E	8.12	10.27
4_C	3.75	1.39
4_D	8.16	5.70
4_E	8.98	7.52
5_C	6.93	21.26
5_D	7.10	17.75
5_E	6.64	18.20
6_C	6.71	13.68
6_D	6.65	12.81
6_E	6.08	11.54

Figure 18

Bending test results (the number in the specimen serial number refers to the welding process)

The shear test design (Figure 19 left side) was a quasi-pure shear test with an extremely small span bending, until the first crack. In the present case, even in a 3-point shear with minimal support spacing, process #1 proved to be the most flexible, with a displacement of 4.53 mm. Compared with this data, the average displacement differences for the other processes were within 1 mm, ranging from 2.63 to 3.36 mm.

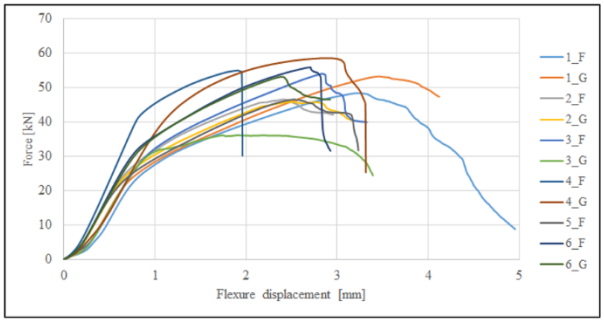

Specimen serial number	Force [kN]	Displacement [mm]
1_F	48.33	4.94
1_G	53.20	4.11
2_F	46.49	2.95
2_G	45.84	3.16
3_F	54.00	3.32
3_G	36.11	3.39
4_F	54.84	1.95
4_G	58.54	3.30
5_F	46.53	3.22
6_F	55.87	2.92
6_G	53.08	2.92

Figure 19

Shear test results (the number in the specimen serial number refers to the welding process)

Again, process #4 proved to be the most rigid, but these specimens also sustained the highest shear forces, averaging 56.7 kN. Values around 50 kN or above were also obtained for processes #6 and #1, while processes #2 and #3 showed favorable values in previous destructive tests and ended up at the bottom of the list with values of 45-46 kN.

Conclusions

The test results show that even with the most advanced technological discipline, joint welding of different materials, without changing their mechanical properties, is difficult. Because the rail material is conditionally weldable when preheating and interpass temperatures are used to prevent cracking, annealing of the Hardox steels is expected. Even when using a welding material with a higher elongation yield strength than the base material, welded joints cannot achieve elongation values close to those of the base material, and tensile strength values are significantly lower, around 60%. Given the preceding findings, hardened fine-grained plates should be classified by traffic load category, with welds specified for the appropriate rail grades. Processes #2 and #3 gave the best results, as determined only by laboratory tests. Based to the structural design and track forces, tensile strength may be the most important criterion, with process #3 coming out on top. However, when considering in-track repairability (e.g., flame cutting) and plate annealing, process #2 performed well. The plates may be suitable for use with R260 rail quality, but with R400 HT rails, despite the advantageous shear values, the system can become extremely rigid and inflexible, increasing the risk of failure when connecting systems of different geometries and weights. Using a hard-facing layer on R400 HT rails should always be avoided. Because the system's components have different degrees of flexibility, a more rigid and expensive concrete plate design can provide a longer service life than a traditional ballasted bed design. The tests should be supplemented in the future with additional laboratory tests, such as fatigue or microstructural tests, to help determine the application conditions for hardened fine-grained plates or Hadfield steels, because Hadfield steels have a very good hardness distribution in the HAZ and base material, as well as successful shear test results.

Acknowledgement

The research was supported by SIU Foundation’s project 'Sustainable railways – Investigation of the energy efficiency of electric rail vehicles and their infrastructure'. The publishing of the paper didn’t receive neither financial support, nor financing of the article process charge.

References

[1] B. Ramazan, R. Mussaliyeva, Z. Bitileuova, V. Naumov, I. Taran. Choosing the logistics chain structure for deliveries of bulk loads: Case study of the Republic Kazakhstan. Naukovyi Visnyk Natsionalnoho Hirnychoho Universytetu, Vol. 2021(3), 2021, pp. 142-147, https://doi.org/10.33271/nvngu/2021-3/142

[2] G. Nugymanova, M. Nurgaliyeva, Z. Zhanbirov, V. Naumov, I. Taran. Choosing a servicing company's strategy while interacting with freight owners at the road transport market. Naukovyi Visnyk Natsionalnoho Hirnychoho Universytetu, Vol. 2021(1), 2021, pp. 204-210, https://doi.org/10.33271/nvngu/2021-1/204

[3] S. Fischer, S. Kocsis Szürke. Detection process of energy loss in electric railway vehicles. Facta Universitatis, Series: Mechanical Engineering, Vol. 21(1), 2023, pp. 81-99, https://doi.org/10.22190/FUME221104046F

[4] A. Kuchak, D. Marinkovic, M. Zehn. Parametric investigation of a rail damper design based on a lab-scaled model. Journal of Vibration Engineering Technologies, Vol. 9, 2021, pp. 51-60, https://doi.org/10.1007/s42417-020-00209-2

[5] A. Kuchak, D. Marinkovic, M. Zehn. Finite element model updating–Case study of a rail damper. Structural Engineering and Mechanics, Vol. 73(1), 2022, pp. 27-35, http://doi.org/10.12989/sem.2020.73.1.027

[6] S. Fischer. Geogrid reinforcement of ballasted railway superstructure for stabilization of the railway track geometry–A case study. Geotextiles and geomembranes, Vol. 50(5), 2022, pp. 1036-1051, https://doi.org/10.1016/j.geotexmem.2022.05.005

[7] L. Ézsiás, R. Tompa, S. Fischer. Investigation of the Possible Correlations Between Specific Characteristics of Crushed Stone Aggregates. Spectrum of Mechanical Engineering and Operational Research, Vol. 1(1), 2024, pp. 10-26

[8] A. Miltenović, M. Banić, D. Stamenković, M. Milošević, M. Tomić. Determination of friction heat generation in wheel-rail contact using FEM. Facta Universitatis, Series: Mechanical Engineering, Vol. 13(2), 2015, pp. 99-108

[9] M. Kurhan M., D. Kurhan, M. Husak, N. Hmelevska. Increasing the Efficiency of the Railway Operation in the Specialization of Directions for Freight and Passenger Transportation. Acta Polytechnica Hungarica, Vol. 19(3), 2022, pp. 231-244, https://doi.org/10.12700/APH.19.3.2022.3.18

[10] M. Kurhan, D. Kurhan. Problems of providing international railway transport. MATEC Web of Conf., 230, 2018, 01007. https://doi.org/10.1051/matecconf/201823001007

[11] L. Ezsias, A. Brautigam, S. Kocsis Szurke, S. Szalai, S. Fischer. Sustainability in railways–a review. Chemical Engineering Transactions, Vol. 107, 2023, pp. 7-12, https://doi.org/10.3303/CET23107002

[12] D. Kurhan. Entropy Application for Simulation the Ballast State as a Railway Element. Acta Polytechnica Hungarica, Vol. 20(1), 2023, pp. 63-77, https://doi.org/10.12700/APH.20.1.2023.20.5

[13] J. Liu, M. Sysyn, Z., Liu, L. Kou. Wang, P. Studying the Strengthening Effect of Railway Ballast in the Direct Shear Test due to Insertion of Middle-size Ballast Particles. Journal of Applied and Computational Mechanics, Vol. 8(4), 2022, pp. 1387-1397, https://doi.org/10.22055/jacm.2022.40206.3537

[14] S. Fischer. Evaluation of inner shear resistance of layers from mineral granular materials. Facta Universitatis, Series: Mechanical Engineering, 2023, https://doi.org/10.22190/FUME230914041F

[15] S. Fischer. Investigation of the horizontal track geometry regarding geogrid reinforcement under ballast. Acta Polytechnica Hungarica, Vol. 19(3), 2022, pp. 89-101, https://doi.org/10.12700/APH.19.3.2022.3.8

[16] L. Kou, M. Sysyn, J. Liu, O. Nabochenko, Y. Han, D. Peng, S. Fischer. Evolution of Rail Contact Fatigue on Crossing Nose Rail Based on Long Short-Term Memory. Sustainability, Vol. 14(24), 2022, 16565, https://doi.org/10.3390/su142416565

[17] B. An, P. Wang, J. Xiao, J. Xu, R. Chen. Dynamic response of wheel-rail interaction at rail weld in high-speed railway. Shock and Vibration, 2017, 5634726, https://doi.org/10.1155/2017/5634726

[18] Y. Gao, J. Xu, P. Wang, Y. Liu. Effect of surface hardening on dynamic frictional rolling contact behavior and degradation of corrugated rail. Shock and Vibration, 2019, 5493182, https://doi.org/10.1155/2019/5493182

[19] Y. Xiang, D. Yu, X. Cao, Y. Liu, J. Yao. Effects of thermal plasma surface hardening on wear and damage properties of rail steel. Proceedings of the Institution of Mechanical Engineers, Part J: Journal of Engineering Tribology, Vol. 232(7), 2018, pp. 787-796, https://doi.org/10.1177/1350650117729073

[20] V. Barna, A. Brautigam, B. Kocsis, D. Harangozó, S. Fischer. Investigation of the Effects of Thermit Welding on the Mechanical Properties of the Rails. Acta Polytechnica Hungarica, Vol. 19(3), 2022, pp. 37-49, https://doi.org/10.12700/APH.19.3.2022.3.4

[21] S. Fischer, D. Harangozó, D. Németh, B. Kocsis, M. Sysyn, D. Kurhan, A. Brautigam. Investigation of Heat-Affected Zones of Thermite Rail Weldings. Facta Universitatis, Series: Mechanical Engineering, 2023, https://doi.org/10.22190/FUME221217008F

[22] A. Brautigam, S. Szalai, S. Fischer. Investigation of the application of austenitic filler metals in paved tracks for the repair of the running surface defects of rails considering field tests. Facta Universitatis, Series: Mechanical Engineering, 2023, https://doi.org/10.22190/FUME230828032B

[23] R. Zellagui, L. Hemmouche, H. Ait-Sadi, A. Chelli. Effect of Element Addition, Microstructure Characteristics, Mechanical Properties, Machining and Welding Processes of the Hadfield Austenitic Manganese Steel.

Archives of Metallurgy and Materials, Vol. 67, 2022, pp. 863-868, https://doi.org/10.24425/amm.2022.139676

[24] S. E. Pratiwi, A. A. Supriyanto, D. P. B. Aji. The influence of heat rate and austenitization temperature on microstructure and hardness of Hadfield steel. Sinergi, Vol. 27(2), 2023, pp. 241-248, https://doi.org/10.22441/sinergi.2023.2.012

[25] B. Venturelli, G. Tressia, E. Albertin (2022) Effect of manganese content on the wear resistance and impact properties of Hadfield steel, 51st Melting, Refining & Casting Conference, June 7-9, 2022. São Paulo, Brazil

[26] K. Ligier, M. Zemlik, M. Lemecha, Ł. Konat, J. Napiórkowski. Analysis of Wear Properties of Hardox Steels in Different Soil Conditions. Materials, Vol. 15(21), 2022, 7622, https://doi.org/10.3390/ma15217622

[27] B. Gallina, L. V. Biehl, J. L. B. Medeiros, J. de Souza. The influence of different heat treatment cycles on the properties of the steels HARDOX® 500 and STRENX® 700. Revista Liberato, Vol. 21(35), 2020, pp. 67-74, https://doi.org/10.31514/rliberato.2020v21n35.p67

[28] É. S. Passari, H. J. Amorim, A. J. Souza. Multi-objective optimization of cutting parameters for finishing end milling Hardox® 450. ITEGAM-JETIA, Vol. 8(34), 2022, pp. 20-28, https://doi.org/10.5935/jetia.v8i34.805

[29] European Committee for Standardization, 2011, EN 13674-1:2011, Railway applications. Track. Rail. Part 1: Vignole railway rails 46 kg/m and above, 123 p.

[30] International Organization for Standardization, 2023, ISO 4063:2023, Welding, brazing, soldering and cutting – Nomenclature of processes and reference numbers 25 p.

[31] European Committee for Standardization, 2014, EN 14700:2014, Welding and allied processes, 14 p.

[32] European Committee for Standardization, 2011, EN ISO 9015-1:2011, Destructive tests on welds in metallic materials – Hardness testing, 19 p.

[33] European Committee for Standardization, 2014, EN ISO 6507-1, Metallic materials. Vickers hardness test, 40 p.

[34] International Organization for Standardization, 2013, ISO 18265:2013, Metallic materials – Conversion of hardness values 90 p.